First-principles investigation of thickness-dependent electrical resistivity for low-dimensional interconnects

Benoit Van Troeye, Kiroubanand Sankaran, Zsolt Tokei, Christoph Adelmann, and Geoffrey Pourtois
Imec, 3001 Leuven, Belgium

(Received 13 April 2023; revised 27 July 2023; accepted 25 August 2023; published 11 September 2023)

The relentless miniaturization of transistors drives the search for alternative metals to copper for low-dimension interconnects. Indeed, some elementary metals, like ruthenium, become less resistive than copper at low dimensions, leading to smaller losses in the connection lines. For most parts, such knowledge is still lacking for binary metals and other alloys. In this work, we carry such an investigation based on first principles, combining electron-phonon and surface scatterings in the relaxation time approximation of Boltzmann's transport equation. We discuss the validity of different proxies of the resistivity at low dimensions (both for thin films and rectangular nanowires), including the so-called $\rho\lambda$ product, that do not require the computation of the electron-phonon relaxation time. We then identify a few promising binary systems that can in principle compete with copper at low dimensions, namely NiAl, RuAl, and Cu_3Al. Finally, we derive on the way the analytical solution of Boltzmann's transport equation for rectangular nanowires.

DOI: 10.1103/PhysRevB.108.125117

I. INTRODUCTION

In order to keep losses and the RC time constant of the chip in check, the resistivity of connection lines—also referred to as the interconnect—must be minimized [1,2]. While copper does the job for thick lines, its resistivity significantly increases upon dimension reduction. This observation can be rationalized based on the Mayadas-Shatzkes model [3] where this increase is attributed to surface scatterings and to the reduction of grain size upon growth of the thin film (i.e., increase of grain scatterings). In order to minimize this effect, one needs either to find a way to enlarge the grain size in the copper thin films (through process) [4] or an alternative material that shows a slower increase of resistivity with reducing dimensions, as well as a sufficiently low bulk resistivity [1,5–10]. In this work, we discuss how ab initio computations can provide insights for the latter road.

The bulk resistivity of a (perfect) single crystal is limited by electron-phonon scatterings, and can be estimated combining first-principles calculations and Boltzmann's transport equation (BTE) [11]. While the latter can be in principle solved iteratively [11,12], the relaxation time approximation, either in its self-energy (SERTA) or its momentum (MRTA) form [11], is generally performed to combine it with surface scatterings. In either way, the BTE must be fed with very dense electron and phonon meshes to converge the electrical resistivity, far too dense to compute in a brute force manner *ab initio*. To overcome this limitation, the phonons are generally interpolated using a Fourier interpolation while the electrons are interpolated using either Wannier functions (EPW [13] or PERTURBO [14]) or a non-self-consistent cycle (ABINIT [15–20]) to reach the desired mesh density. The bulk resistivity of elementary metals have been successfully investigated with those approaches [21–24]. Even with these interpolation schemes, such computations remain computationally challenging on systems larger than a dozen of atoms. It is then useful to introduce proxies—that are independent of the relaxation time—to estimate the resistivity increase at low dimensions in a given material and to compare it to copper.

In that regard, the most popular approach relies on the so-called $\rho\lambda$ quantity [5,7,25,26] that only depends on the electron velocities around the Fermi level, with different variants. More recent proxies also include an angular dependency [9] (r_{film}) for thin films and rectangular nanowires. Their derivations however suppose, to the best of our knowledge, a constant relaxation time approximation, i.e., no wave vector nor band index dependency, which needs to be demonstrated. A more formal derivation way is still lacking.

In this work, we investigate in a first phase the resistivity of elementary metals using first-principles methods, and highlight the importance of the growth orientation on their low-dimension resistivity. We derive analytically the origin of the $\rho\lambda$ product, highlighting the presence of a missing term related to the growth orientation in the expression and leading to a new definition $\rho\lambda(\hat{u}_n)$. We then discuss the validity of resistivity proxies by comparing them with first-principles calculations of the resistivity increase at low dimensions for a set of binary metals. We find that both the $\rho\lambda(\hat{u}_n)$ and r_{film} are suited to predict the resistivity increase at low dimension. We extend this analysis to rectangular nanowires, deriving the analytical expression of Boltzmann's transport equation with 2D confinement, as well as the corresponding proxy. In parallel, we investigate the low-dimension resistivity of a few binary metals. Among the investigated materials, NiAl, RuAl, and Cu_3Al are showing the most interesting perspectives for an interconnect application.

II. THEORY

The conductivity tensor $\sigma_{\alpha\beta}$—the inverse of the resistivity tensor $\rho_{\alpha\beta}$—can be obtained from the relaxation-time

 ©2023 American Physical Society

approximation [11]:

$$\sigma_{\alpha\beta} = [\underline{\underline{\rho}}^{-1}]_{\alpha\beta} = -\frac{n_s e^2}{N_{\mathbf{k}}\Omega} \sum_{n,\mathbf{k}} \frac{\partial f_{n,\mathbf{k}}}{\partial \varepsilon} v^{\alpha}_{n,\mathbf{k}} v^{\beta}_{n,\mathbf{k}} \tau_{n,\mathbf{k}}, \quad (1)$$

where n is the band index, $\mathbf{k}$ is the electronic wave vector, n_s is the band occupation (1 if spin or fully relativistic treatment of spin-orbit coupling are considered, 2 otherwise), e the electron charge, $N_{\mathbf{k}}$ the total number of k points, Ω the volume of the primitive cell. $\partial f_{n\mathbf{k}}/\partial \varepsilon$ is the derivative with respect to energy of the Fermi-Dirac distribution for the electronic state $(n, \mathbf{k})$. $v^{\alpha}_{n,\mathbf{k}} = 1/\hbar \times \partial \epsilon_{n,\mathbf{k}}/\partial k^{\alpha}$ is the velocity in the cartesian direction α, with $\hbar$ is the reduced Planck constant and $\epsilon_{n,\mathbf{k}}$ the eigenenergy state. Finally, $\tau_{n,\mathbf{k}}$ is the electron-phonon relaxation time which can be estimated, for example, in SERTA:

$$\frac{1}{\tau_{n\mathbf{k}}} = \frac{2\pi}{\hbar} \sum_{m\mathbf{q}} \int_{\mathrm{BZ}} \frac{d\mathbf{q}}{\Omega_{\mathrm{BZ}}} |g_{mn\nu}(\mathbf{k},\mathbf{q})|^2 h_{\nu,mn}(\mathbf{k},\mathbf{q}) \quad (2)$$

or MRTA,

$$\frac{1}{\tau_{n\mathbf{k}}} = \frac{2\pi}{\hbar} \sum_{m\mathbf{q}} \int_{\mathrm{BZ}} \frac{d\mathbf{q}}{\Omega_{\mathrm{BZ}}} |g_{mn\nu}(\mathbf{k},\mathbf{q})|^2 h_{\nu,mn}(\mathbf{k},\mathbf{q}) \times \left(1 - \frac{\mathbf{v}_{n,\mathbf{k}}.\mathbf{v}_{m,\mathbf{k+q}}}{|v_{n,\mathbf{k}}|^2}\right), \quad (3)$$

where Ω_{BZ} is the volume of the Brillouin zone (BZ), $h_{\nu,mn}(\mathbf{k},\mathbf{q})$ is the electron-phonon coupling matrix element between the electronic states $(n, \mathbf{k})$ and $(m, \mathbf{k}+\mathbf{q})$ through the phonon mode $(\nu, \mathbf{q})$. The $h_{\nu,mn}$ factor selects the possible transitions as follows:

$$h_{\nu,mn}(\mathbf{k},\mathbf{q}) = (n_{\mathbf{q},\nu} + f_{m,\mathbf{k+q}})\delta(\epsilon_{n,\mathbf{k}} - \epsilon_{m,\mathbf{k+q}} + \omega_{\mathbf{q},\nu}) + (n_{\mathbf{q},\nu} + 1 - f_{m,\mathbf{k+q}})\delta(\epsilon_{n,\mathbf{k}} - \epsilon_{m,\mathbf{k+q}} - \omega_{\mathbf{q},\nu}), \quad (4)$$

where $\omega_{\mathbf{q},\nu}$ is the phonon frequency of mode ν at the phonon wavevector $\mathbf{q}$, δ stands for the Kronecker delta and $n_{\nu\mathbf{q}}$ is the Bose-Einstein distribution.

Equation (1) gives the conductivity of a perfect bulk crystal from Boltzmann's transport equation in the relaxation time approximation. With this approximation, one can also solve such an equation including surface scatterings [9,25,27,28]. In a first phase, we consider the finite dimension along the growth orientation of the film $\hat{u}$ with h thickness. In the case of fully diffuse surfaces, Eq. (1) is still valid upon the introduction a modified scattering time:

$$\tau_{n\mathbf{k}}(h,\hat{u}) = \tau^{\mathrm{ep}}_{n\mathbf{k}}\left(1 + \frac{|\boldsymbol{\lambda}_{n\mathbf{k}}.\hat{u}|}{h}\left[1 - \exp\left\{\frac{-h}{|\boldsymbol{\lambda}_{n\mathbf{k}}.\hat{u}|}\right\}\right]\right), \quad (5)$$

where $\tau^{\mathrm{ep}}_{n\mathbf{k}}$ is the electron-phonon relaxation time and $\hat{u}$ is the film orientation and $\lambda^{\alpha}_{n\mathbf{k}} = v^{\alpha}_{n\mathbf{k}}\tau_{n\mathbf{k}}$ the mean-free path of a given electron mode. Effectively, the surface scattering leads to a reduction of the relaxation time of the electron modes with an out-of-plane component, and leaves unaffected the ones propagating in-plane. The surface specularity is introduced using the parameter p which expresses the fraction of electron that are scattered specularly by the surface; the relaxation time becomes

$$\frac{\tau_{n\mathbf{k}}}{\tau^{\mathrm{ep}}_{n\mathbf{k}}} = 1 + \frac{|\boldsymbol{\lambda}_{n\mathbf{k}}.\hat{u}|}{h} \frac{1-p}{1 - p\exp\left(\frac{-h}{|\boldsymbol{\lambda}_{n\mathbf{k}}.\hat{u}|}\right)}\left[1 - \exp\left\{\frac{-h}{|\boldsymbol{\lambda}_{n\mathbf{k}}.\hat{u}|}\right\}\right]. \quad (6)$$

When $p = 0$, the surface is fully diffuse and one recovers Eq. (5) where the resistivity increase is the most important, while in the case of fully reflective surfaces, there is no impact of the film thickness on the resistivity. Note that the specularity coefficient p is generally assumed to be a constant, i.e., independent of the electron momentum.

Based on Eqs. (1) and (5), the electrical conductivity at low dimensions results from the interplay between two quantities, namely, (i) the bulk conductivity and (ii) a rescaling factor related to the electron mean-free path along the thin film growth orientation. The more electrons are parallel to this surface, the further the electrical conductivity downscales with decreasing dimensions. This downscaling is in consequence directly related to the Fermi surface anisotropy of the material under question.

Since electron-phonon computations are relatively costly, estimating the increase of resistivity at low dimensions with only knowledge of the electronic band structure is useful. In this view, the $(\rho\lambda)^{-1}$ product [5,7,26] has been introduced as a proxy to predict the resistivity variation at low dimension:

$$\frac{1}{\rho\lambda} = -\frac{n_s e^2}{N_{\mathbf{k}}\Omega} \sum_{n,\mathbf{k}} \frac{\partial f_{n,\mathbf{k}}}{\partial \varepsilon} \frac{|\mathbf{v}_{n,\mathbf{k}}.\hat{n}|^2}{|\mathbf{v}_{n,\mathbf{k}}|}, \quad (7)$$

where $\hat{n}$ is the in-plane transport direction. Based from Eq. (5), we can demonstrate formally its origin. Taylor-expanding the exponential close to $h = 0$ in the case of electron modes nearly aligned to the surface orientation vector, one finds

$$\tau_{n\mathbf{k}}(h,\hat{u}) \approx \tau^{\mathrm{ep}}_{n\mathbf{k}}(h,\hat{u}) \frac{h}{2|\boldsymbol{\lambda}_{n\mathbf{k}}.\hat{u}|} + O(h^3), \quad (8)$$

where the zero- and first-order terms of the Taylor expansion cancel out. Reinjecting Eq. (8) in Eq. (1), recalling that $\lambda^{\alpha}_{n\mathbf{k}} = v^{\alpha}_{n\mathbf{k}}\tau_{n\mathbf{k}}$, one finds

$$\sigma_{\alpha\beta}(h \approx 0) \approx -\frac{h n_s e^2}{N_{\mathbf{k}}\Omega} \sum_{n,\mathbf{k}} \frac{\partial f_{n,\mathbf{k}}}{\partial \varepsilon} \frac{|\mathbf{v}_{n,\mathbf{k}}.\hat{e}|^2}{2|\mathbf{v}_{n\mathbf{k}}||\hat{v}_{n\mathbf{k}}.\hat{u}|}, \quad (9)$$

where we have introduced $\hat{v}_{n\mathbf{k}}$ the unitary direction vector of the electron velocity $\hat{v}_{n,\mathbf{k}} = \mathbf{v}_{n,\mathbf{k}}/|\mathbf{v}_{n,\mathbf{k}}|$. This expression diverges when $|\hat{v}_{n\mathbf{k}}.\hat{u}| \to 0$, and we introduce thus an angular cutoff θ:

$$\frac{1}{\rho\lambda(\hat{u}_n)} = -\frac{n_s e^2}{N_{\mathbf{k}}\Omega} \sum_{|\hat{v}_{n\mathbf{k}}.\hat{u}|>\theta} \frac{\partial f_{n,\mathbf{k}}}{\partial \varepsilon} \frac{|\mathbf{v}_{n,\mathbf{k}}.\hat{n}|^2}{2|\mathbf{v}_{n\mathbf{k}}||\hat{v}_{n\mathbf{k}}.\hat{u}|}. \quad (10)$$

This expression is extremely similar to the approximation $(\rho\lambda)^{-1}$ [Eq. (7)], albeit for the $1/|\hat{v}_{n\mathbf{k}}.\hat{u}|$ factor that introduces the Fermi surface anisotropy. One can directly note that this approximation is unsuited for electrons whose wave vector is perpendicular to the film orientation (e.g., 2D material). A more suited approximation would then be

$$\sigma_{\alpha\beta}(h \approx 0) \approx \sigma^{\parallel} - \frac{h n_s e^2}{N_{\mathbf{k}}\Omega} \sum_{|\hat{v}_{n\mathbf{k}}.\hat{u}|>\theta} \frac{\partial f_{n,\mathbf{k}}}{\partial \varepsilon} \frac{|\mathbf{v}_{n,\mathbf{k}}.\hat{n}|^2}{2|\mathbf{v}_{n\mathbf{k}}||\hat{v}_{n\mathbf{k}}.\hat{u}|}, \quad (11)$$

where we have introduced

$$\sigma^{\parallel} = -\frac{n_s e^2}{N_{\mathbf{k}}\Omega} \sum_{|\hat{v}_{n\mathbf{k}}.\hat{u}|<\theta} \frac{\partial f_{n,\mathbf{k}}}{\partial \varepsilon} |\mathbf{v}_{n,\mathbf{k}}.\hat{n}|^2 \tau_{n\mathbf{k}}. \tag{12}$$

From this expression, it appears that, in order to achieve the lowest resistivity increase in a thin film, one has either to find a material with a preferential transport perpendicular to the film thickness (typically a 2D material) or to identify a material with a small $\rho\lambda(\hat{u}_n)$ product, which is independent of the relaxation time (and thus cheaper to compute). In that respect, Kumar *et al.* introduced the scaling coefficient $r_{\text{film}}(\hat{u})$ [9]:

$$\frac{1}{r_{\text{film}}} = -\frac{3n_s e^2}{8N_{\mathbf{k}}\Omega} \frac{\left(\sum_{n\mathbf{k}} |\mathbf{v}_{n,\mathbf{k}}.\hat{n}|^2 \partial f_{n,\mathbf{k}}/\partial \varepsilon\right)^2}{\sum_{n\mathbf{k}} |\mathbf{v}_{n,\mathbf{k}}.\hat{n}|^2 |\mathbf{v}_{n,\mathbf{k}}.\hat{u}| \partial f_{n,\mathbf{k}}/\partial \varepsilon}, \tag{13}$$

derived from Eq. (5) neglecting the exponential term and supposing a constant electron-phonon time. We will discuss the validity of these different proxies to predict the increase of resistivity at low dimensions in Sec. V. Note nevertheless that achieving a low increase of resistivity [small $\rho\lambda(\hat{u}_n)$] should not come at a too big expanse on the bulk resistivity if one wants to compete with copper. We will discuss the importance of these two different terms (bulk resistivity and resistivity increase) in the incoming sections for both thin films and rectangular nanowires.

III. COMPUTATIONAL DETAILS AND BENCHMARKS ON ELEMENTARY METALS

In a first phase, we investigate the electrical resistivity of an arbitrary set of elementary metals in their experimental crystalline structures reported at room temperature [29], i.e., Cu, Ag, Al, Au, Pd, and Ir in their FCC phases, Mo and W in their BCC phases, Ru in its hexagonal phase. The objective of this analysis is, on the one hand, to characterize the expected accuracy of the present methodology (for the subsequent binary investigation), and on the other hand to evaluate their increase of resistivity at low dimensions.

Density functional theory (DFT) computations are performed using the ABINIT [15–17,30] software package, with the LDA exchange-correlation functional and with norm-conserving ONCVPSP scalar-relastivistic pseudopotentials [31], available at the PSEUDODOJO website (v0.4.1) [32]. For W, we also use a fully relativistic pseudopotential instead for sake of a later comparison between these two descriptions of spin-orbit coupling. The stringent plane-wave cut-off energies (0.4 mHa/atom convergence) are used, as suggested by the pseudopotential documentation files for each of the considered element. To enforce continuity of stress with varying the unit cell volume, a plane-wave cut-off smearing of 0.5 Ha is applied during relaxation, and is kept in all the consecutive computations for sake of consistency (phonons and electron-phonon). A Fermi-Dirac smearing of the electronic occupation ranging from 0.001 to 0.005 Ha and $18\times18\times18$ k-point mesh for cubic systems (except Pd, going up to $24\times24\times24$) and a $12\times12\times8$ for hexagonal systems, respectively, are found to lead to a satisfactory precision (0.5 mHa/atom on the total energy). The phonon and subsequent electron-phonon computations are performed on the corresponding relaxed structures.

TABLE I. Electrical resistivity computed in this work from MRTA (ρ^{MRTA}), SERTA (ρ^{SERTA}) compared to experiments (ρ^{exp}) [4,34–39], and Tong *et al.* ($\rho^{\text{SERTA}}_{\text{Tong}}$) [21] at 300 K.

Metal	Temperature (K)	ρ^{MRTA} [$\mu\Omega$ cm]	ρ^{SERTA} [$\mu\Omega$ cm]	$\rho^{\text{SERTA}}_{\text{Tong}}$ [$\mu\Omega$ cm]	ρ_{exp} [$\mu\Omega$ cm]
Cu	293	1.68	1.97	1.90	1.52
Ag	293	1.52	1.51	1.60	1.49
Au	293	2.23	2.23	2.75	2.22
Al	293	2.48	3.01	2.97	2.62
Ir	293	4.13	3.84	–	5.00
Pd	300	7.81	7.68	12.20	9.76
Mo	293	5.52	6.04	–	5.45
W*	293	4.83	5.10	–	5.30
Ru	300	5.79	5.51	–	7.02

*with spin-orbit coupling.

For the phonon mesh, the Brillouin zone is sampled using a $9\times9\times9$ and $6\times6\times4$ zone-centered q-point mesh for cubic systems and Ru, respectively. Phonon-limited electrical resistivities are then estimated at 300 K using both the SERTA and MRTA approximations, and using a non-self-consistent and a Fourier interpolation schemes for the electrons and the phonons [19,20], respectively. Tetrahedron integration is used both for the relaxation time and conductivity computations. Convergence studies for these elementary metals with respect to this dense interpolated k-point mesh are performed up to 10%, leading to a q-point mesh twice as dense along each direction. They are reported in Figs. S1 to S3 of Ref. [33]. It is found that for most of the considered metals, the resistivity computed by the internal BTE solver of ABINIT varies to a good approximation exponentially: in the following, we use the resistivity extrapolated asymptotically for sake of comparison to experiments. This leads to resistivity values converged within 1% with respect to the asymptotic value. Note that other choices of extrapolation functions are legitimate, for, e.g., $1/k$, which leads to 3% to 10% lower asymptotic resistivity depending on the considered material.

The corresponding experimental resistivities are reported in literature at temperatures ranging from 273.15 to 300 K [4,34–39]. For sake of comparison, we extrapolate either the experimental values using the experimental temperature coefficient—when available- or the computed resistivities using the value obtained at 214 K. Not taking into account of such subtle variations change the resistivity by ∼2.5%, to be considered alongside the experimental error bar (typically 0.5%–2% [39]), and the eventual residual contribution from grain scatterings when the system is not a single crystal (see Table I). For instance, for Al, Ag, or Cu, differences of 6.4%–12% are reported between single and polycrystalline crystals resistivities [4,34]. The computed values are compared to experiments in Fig. 1 and Table I; they show a good agreement between computations and experiments, especially when single-crystal data are experimentally reported. For the other polycrystalline crystals, namely, Ir and Pd, some discrepancies can be explained by grain scattering contributions.

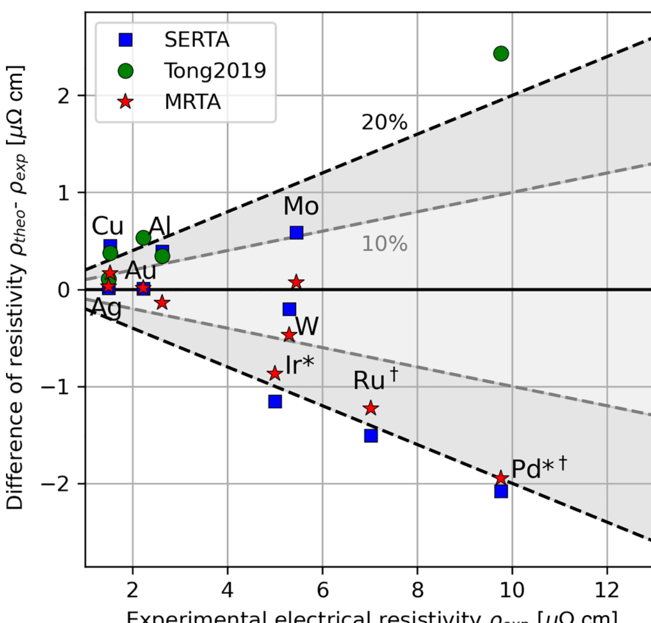

FIG. 1. Comparison between computed bulk electrical resistivity at room temperature using SERTA (blue square) or MRTA (red star) and experimental ones. The results of Tong *et al.* [21] are also shown using green disks. For sake of legibility, the difference between theoretical and experimental resistivities is shown on the y axis, as function of the experimental one. The dash lines correspond to $\pm10\%$ and $\pm20\%$ error bars. The experimental resistivity of metals labeled with an asterisk are measured on polycrystalline samples. For Ru and Pd, denoted with the † symbol, the results are reported for 300 K and are averaged over the principal crystalline directions for the former.

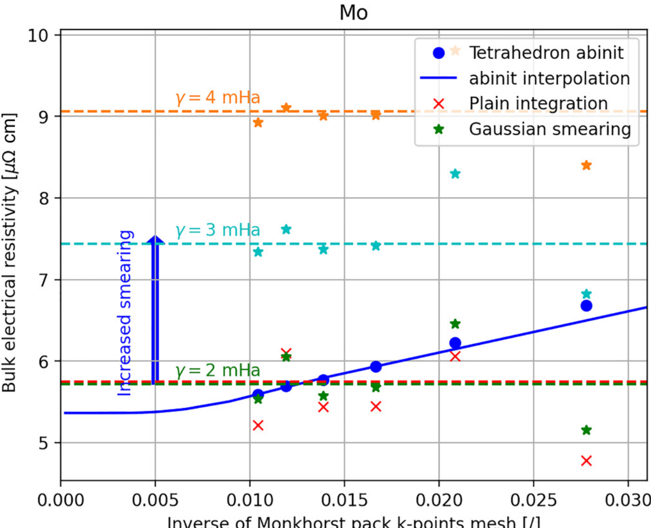

FIG. 2. Convergence study of the bulk electrical resistivity of Mo as function of the inverse of k-point mesh density (corresponding k-point mesh is $n^{-1} \times n^{-1} \times n^{-1}$) for different integration techniques for the resistivity, i.e., blue disks for tetrahedron, red crosses for plain integration and stars for Gaussian smearing. The mean value of the four first points is shown as dash lines. γ corresponds to the smearing value for the Gaussian broadening.

For Pd, we suspect that most of the deviation arises from the treatment of spin-orbit coupling: the inclusion of fully relativistic pseudopotentials and corresponding corrections leads to drastic changes in its electronic band structure close to the Fermi level (see Fig. S4). For other atomic species such as Au, W, or Ir, although being heavier elements, we do not observe such an impact and expect thus much less sensitivity on the resistivity. To further assess this, we compute the electrical resistivity of W using both scalar relativistic and fully relativistic pseudopotentials coupled for the second case with spin-orbit coupling. We use the corresponding relaxed crystalline and phonon band structures. The change in term of resistivity, going from scalar to fully relativistic, is found to be $\sim$3%, i.e., quite small compared to other approximations (e.g., SERTA versus MRTA, see later). This motivated us to remain at the scalar-relativistic treatment of spin-orbit coupling in the following for sake of consistency and computational time.

Comparing now the relaxation time approximations for Boltzmann's transport equations, i.e., SERTA and MRTA, we observe that MRTA (6% relative error) performs slightly better than SERTA (12% relative error) with respect to experiments. The difference is especially large for some outliers ($\sim$20% for Cu and Al), that it has to be kept in mind while moving to the investigation of alternative metals. For sake of comparison, we also show the results of Tong *et al.* obtained using a Wannier interpolation scheme for the electrons at 300 K [21]. A good agreement is observed overall except for Pd. We suspect that these discrepancies originate from the spin-orbit coupling treatment (scalar-relativistic here versus fully relativistic in Ref. [21]), the inclusion of nonlocal contributions for the velocities and the much denser phonon q-point mesh used in this work with respect to theirs ($144\times144\times144$ versus $30\times30\times30$) that all have shown to have a drastic impact on the mobility of semiconductors [40]. Further contributions may originate from different pseudopotentials, exchange-correlation, and smearing value used at the electron-phonon level.

IV. RESISTIVITY OF ELEMENTARY METALS AT LOW DIMENSIONS

In a second phase, we investigate the variation of the electrical resistivity with decreasing thickness; to do so, we need then the velocities on the whole Brillouin zone (surface scattering breaks the symmetry of the system). This could in principle be done directly in ABINIT, but we decide to implement it in python. We regenerate them based on the ABINIT output (the velocities are only printed for the irreductible Brillouin zone) and SPGLIB [41] as post processing:

$$\mathbf{v}_{n\mathbf{k}'} = \left(\underline{\underline{R}}^{-1}\underline{\underline{S}}^{\mathsf{T}}_{\mathbf{k}\mathbf{k}'}\underline{\underline{R}}\right)^{\mathsf{T}}\mathbf{v}_{n\mathbf{k}}, \tag{14}$$

where $\underline{\underline{R}}$ is the lattice vector matrix, $\underline{\underline{S}}$ the matrix operation in real space to go from $\mathbf{k}$ to $\mathbf{k}'$ and T stands for matrix transpose. The conductivity is then computed externally to ABINIT [through Eqs. (1) and (5)] with a plain integration (trapezoidal method) or by adding a Gaussian broadening, similarly to what is done in EPW [11]. As shown in the convergence study in Fig. 2 or the ones in Ref. [33], these values converge asymptotically towards the same values of ABINIT for sufficiently dense interpolated k-point mesh

(see, for example, Figs. S1 to S3), but in a relatively erratic manner. This erraticness is smoothened by the use of a Gaussian smearing, but it introduces a shift of the asymptotic value with respect to the tetrahedron method for too large value of the Gaussian smearing. The values given by those methods have thus to be carefully compared to the ones from the tetrahedron integration; for bulk resistivity, we use the data from the densest k-point mesh for each material, whose corresponding resistivity always falls within 10% of the asymptotic value. We then check the convergence of the resistivity increase at 6 nm with respect to bulk; we observe the same erratic convergence for plain integration that gets smoothen with the Gaussian broadening. To assess the plain integration precision, we compare then to the Gaussian-smeared results for a broadening that reproduce well the bulk resistivity (see Fig. S5); this way we expect an accuracy of $\pm10\%$ for the resistivity increase.

The inclusion of surface scattering requires some knowledge on the preferential orientation of growth of the thin film. For all the elementary metals investigated in this work, the preferential growth orientations are known experimentally: [111] for FCC, [110] for BCC, and [001] for HCP [7]. Note that, in general, the addition of surface scattering in Boltzmann's transport equation leads to a lift of degeneracy between the components of the resistivity tensor in-plane; however, these experimentally observed preferential growth orientations do not lead to such a lift. Due to the high diffusivity of copper [7], a liner is deposited in the interconnects to avoid reliability issues with the surrounding dielectrics. We accounted here for the presence of a 3-nm-thick TaN liner layer grown on top of copper with the same in-plane dimension. The corresponding stack is thus effectively two resistances in parallel, one of copper (that varies with its film thickness) and one of TaN, for which we use an electrical resistivity of 95 $\mu\Omega\,\mathrm{cm}$ extracted from experiments [42]. In practice, the use of a higher resistivity for TaN only weakly impacts the stack resistivity curve, except at extremely low dimensions (<3 nm), where the validity of our approach becomes questionable in any case.[1] The results of our investigations are shown in Fig. 3. As one can see, the Cu + liner becomes more resistive than most of the other elementary metals at low dimensions. Most of the crossings occurs between 20 and 4 nm. This is consistent with experimental observations [7] although the crossing occurs at higher thickness, from 3 to 6 nm, as well as other theoretical works [9]. Note that grain scattering and its corresponding evolution with decreasing dimensions are not included here. These effectively lead to an additional increase of the resistivity [3] compared to the case where only (diffuse) surface scattering is considered. These can be in practice the most critical contributions [3,7], but it is impossible to capture this using a first-principles approach without introducing empirical parameters to the best of our knowledge. Consequently, the results we report here reflect the "best case scenario," namely, the resistivity variation of perfect single-crystals in their thin films forms. Concerning the surface specularity, we find for all the (elementary and binary) metals investigated in this work a (nearly) linear relationship between the resistivity increase and the specularity coefficient (see Fig. S5); in the following, we report the resistivity increase for fully diffuse surfaces (largest resistivity increase), but one can take a $1-p$ fraction of it to get the resistivity increase for the corresponding specularity.

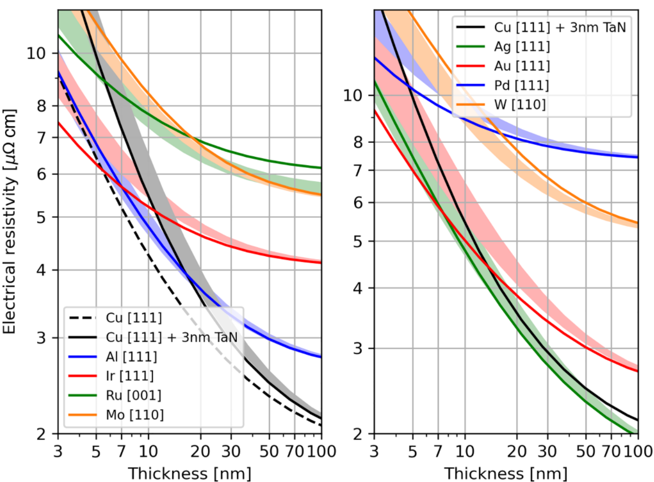

FIG. 3. Variation of the resistivity in elementary metals thin films with decreasing thickness. In full (dash) line, we show the results for a single crystal with a specific growth orientation. Meanwhile, the shaded areas correspond to the interval $[\langle\rho\rangle_{\hat{u}}(h) - S_{\hat{u}}(h), \langle\rho\rangle_{\hat{u}}(h) + S_{\hat{u}}(h)]$, i.e., related to the angular average and variance -indicating how sensitive the thin film is to its change in growth orientation.

In contrast to elementary metals, the preferential growth orientation of thin films made of binary metals is not always known experimentally. It is thus also interesting to evaluate the sensitivity of the resistivity with respect to different surface orientations. To do so, we defined the angular average and standard deviation of the resistivity with respect to the growth orientation as

$$\langle\rho\rangle_{\hat{u}}(h) = \frac{1}{A}\iint \bar{\rho}(h, \hat{u}[\phi, \theta]) \sin\theta \, d\phi d\theta \tag{15}$$

and its variance

$$S^2_{\hat{u}}(h) = \frac{1}{A}\iint (\bar{\rho}(h, \hat{u}[\phi, \theta]) - \langle\rho\rangle_{\hat{u}})^2 \sin\theta \, d\phi d\theta, \tag{16}$$

where A is the angular area defined by all the nonequivalent possible $\hat{u}$ surface vectors, ϕ and θ the azimutal and polar angles, and $\bar{\rho}$ the averaged in-plane eigenvalues of the resistivity tensor for the given surface orientation. This thus takes into account of the eventual symmetry breaking induced by surface scattering. The averaged value provides information on the increase of resistivity if the system would have a (pseudo)isotropic surface, while the interval $[\langle\rho\rangle_{\hat{u}}(h) - S_{\hat{u}}(h), \langle\rho\rangle_{\hat{u}}(h) + S_{\hat{u}}(h)]$ reflects the overall sensitivity of this average with respect to the film growth orientation. For elementary metals, we report in Fig. 3 this interval using shaded area. The well-oriented surface lies, in most of the cases, outside of this interval, especially at low dimensions. For Au, the resistivity spans from 6 to ∼7–8 $\mu\Omega\,\mathrm{cm}$ at 7 nm for example. In other words, the anisotropy of the Fermi surface is critical for most of these elementary metals, and it is thus

[1]No confinement on the electronic band structure is included here.

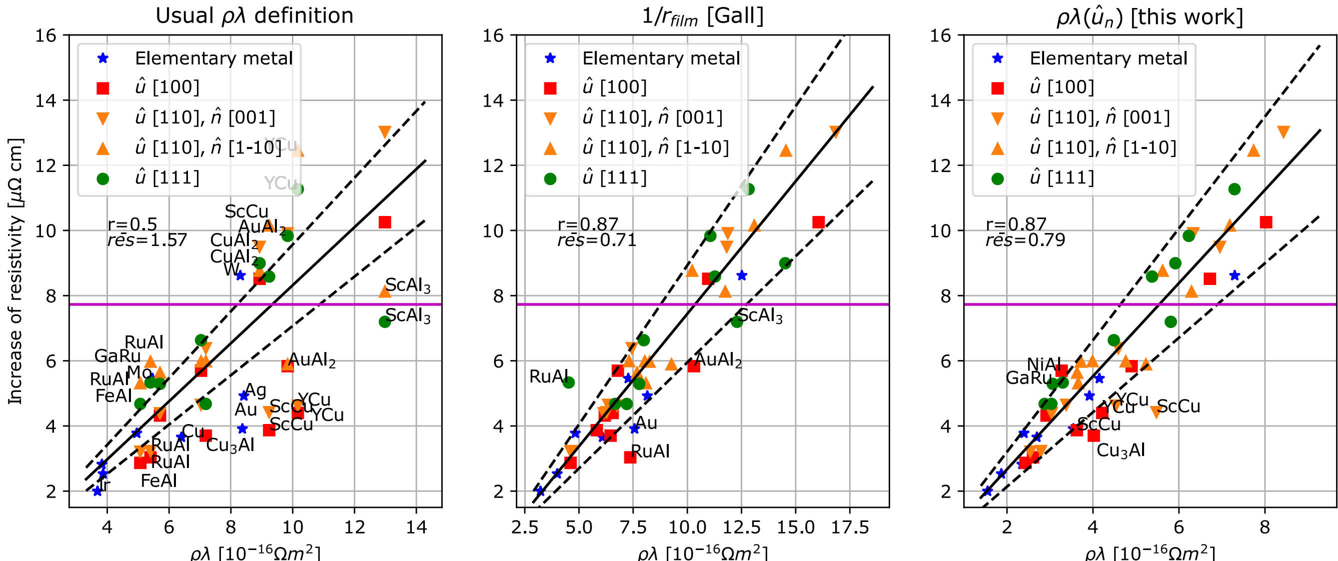

FIG. 4. Increase of resistivity from bulk to 6 nm as function of different $\rho\lambda$ proxies: (left) nondirectional $\rho\lambda$ from Eq. (7) (center) Gall's r_{film} from Eq. (13) and (right) the directional $\rho\lambda(\hat{u}_n)$ from Eq. (9). The full line corresponds to the robust regression using the smooth approximations to the L1-Norm. The Pearson correlation coefficient (r) and the residuals are also shown for sake of information. The pink horizontal line corresponds to the increase of resistivity in the case of Cu + 3 nm TaN.

crucial to specify the film growth orientation used in that context. In consequence, in the following for binary metals, we will always show the resistivity increase for different surface orientations, namely the [100], [110], and [111] (for cubic systems) ones. This does not exclude that the material could grow preferentially along other surface orientations, but this approach provides an insight on the overall sensitivity to growth orientation in the investigated materials.

V. BINARY METALS AND PROXY VALIDITY

Ideally, DFT could be used to screen the most interesting binary metals to compete with Cu for low-dimension interconnects. However, the increase of resistivity at those dimensions is not only caused by surface scatterings but also the reduction of grain size [3,7], which is very difficult to predict from an ab initio point-of-view, as discussed in the previous section. We can nevertheless investigate the magnitude of the surface scattering contribution and see what binary metals show the lowest one, as well as to compare it to (computed) bulk resistivities. Indeed, this latter contribution will nevertheless be limiting for the resistivity, and materials with important increase and large bulk resistivity can be excluded for low-dimension interconnects.

For this investigation, we start from the materials reported as being metallic in the Material Project database [43]. We restrict this analysis to bulk alloys with Cu, Al, Mo, or Ru in their composition and to their corresponding phases located on the convex hull. Interconnect materials require next to a low electrical resistivity, a low sensitivity to electromigration to meet reliability criterion [7]. The extent of the electromigration reflects the binding energy of atoms on surfaces and how keen they are to diffuse during the operation of the transistor. As a consequence, contenders to copper must have a binding/cohesive equal or ideally higher than it. We then ranked the selected candidates based on their cohesive energy and a $\rho\lambda$ product [Eq. (7)]. Candidates with higher cohesive energy and smaller $\rho\lambda$ product than the one of copper were selected. We also excluded materials that either include elements with states close to the Fermi surface that are sensitive to spin-orbit coupling (like Pd and Pt) or whenever magnetism is reported for the corresponding phase on the Material Project database. Due to electron-phonon computational cost, we only consider binaries with 4 or less atoms per unit cell. Furthermore, we excluded any phase that are found to be dynamically unstable based on their phonon band structure (see Figs. S6 to S10). This leaves us with 10 materials for which we followed the same methodology as the one described in Sec. III to compute the phonon-limited resistivity. The coarse k-point and q-point meshes are adapted compared to the elementary metals based on their (relaxed) lattice parameters. For the interpolated meshes, we first compute the electrical resistivity based on relatively coarse k-point and q-point meshes ranging from $36\times36\times36$ to $48\times48\times48$, and $72\times72\times72$ to $96\times96\times96$, respectively, and extrapolate the trend exponentially for denser meshes. We only pushed the convergence up to 10% for the bulk electrical resistivity for the materials that show an extrapolated asymptotic resistivity lower than 8 $\mu\Omega$ cm. The addition of additional points in the convergence is found to always lead to a higher extrapolated resistivity based on the tetrahedron method (see Figs. S11 and S12). We show the convergence studies for the materials with extrapolated resistivity lower than 8 $\mu\Omega$ cm, namely, NiAl, RuAl, Cu_3Al, $AuAl_2$, and $ScAl_3$, in the corresponding figures in Ref. [33].

We compare in Fig. 4 the increase of in-plane resistivity from bulk to 6 nm (SERTA) and the different $\rho\lambda$ proxies defined in Sec. II, computed using the same k-point mesh than the electron-phonon ones and that for different surface orientations. For the directional $\rho\lambda(\hat{u})$, we use a θ

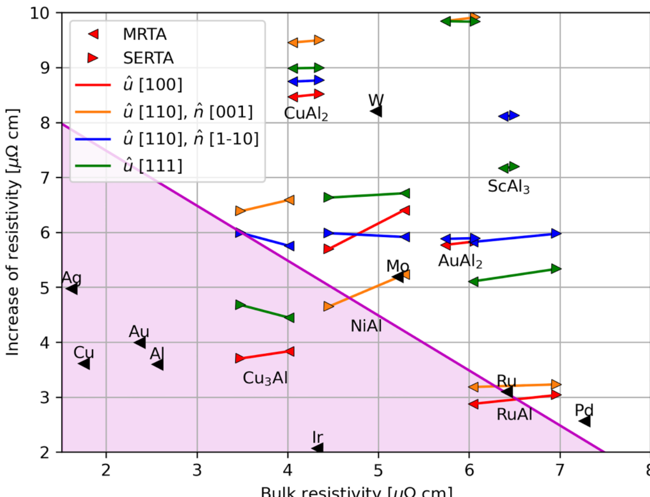

FIG. 5. Increase of resistivity at 6 nm vs bulk resistivity for the different binary metals investigated in this work and for different film growth orientations. Both results obtained using MRTA and SERTA are shown for sake of information. The materials of potential technological interest are the ones that show a cumulative resistivity lower than the one of Cu with liner.

cutoff of 5%. Note that the increase of resistivity is strongly anisotropic: for RuAl, it can varies by a factor ~2 depending on the chosen growth orientation, as expected already from the elementary metals analysis (see Sec. IV). For some of these crystals, the degeneracy in-plane of the resistivity tensor is broken, meaning that we have now to consider the two in-plane components separately: as one can see for $ScAl_3$, the variation is pretty significant, going from 8 to 13 $\mu\Omega$ cm depending on the in-plane direction for transport.

To evaluate the relevance of the different proxies introduced in Sec. II [Eqs. (7), (13), and (9)], we use a robust regression technique using the L1-Norm [44] to fit the resistivity increase versus the proxy, and compute the Pearson correlation coefficient between these two quantities. We find that both the Gall's r_{film} and our directional $\rho\lambda(\hat{u}_n)$ are good estimators of the resistivity increase at low dimensions based on the Pearson correlation coefficient and the residuals of the robust regression. In contrast, the predictive power of $\rho\lambda$ is found to be lacking. This is not an unexpected behavior since by construction, such an approximation cannot capture the Fermi surface anisotropy with respect to the growth orientation, in contrast to r_{film} and $\rho\lambda(\hat{u}_n)$ that have a directional component with respect to it. However, the two latter can be used to screen materials for low-dimension interconnects. The resistivity increase at 7 nm can then be in good approximated as $\Delta\rho \approx 1.43\times10^{16}\rho\lambda(\hat{u}) - 0.19\,\mu\Omega\,\text{cm}$.

In Fig. 5, we compare the bulk resistivity to its increase from bulk to 6 nm for the most interesting materials. Both SERTA and MRTA are here compared; for the bulk resistivity, the variations can be pretty significant: up to 20% for RuAl (see Fig. S13) while the difference is of smaller magnitude for the increase of resistivity (except for NiAl). For a material to be interesting for low-dimension interconnect, it should yield a total resistivity (bulk + increase of resistivity) lower than Cu + liner. As one can see, there are a few candidates that meet this criterion: based on our computations, Cu_3Al, NiAl or RuAl are in principle competing than Cu below 6 nm depending on the growth orientation. NiAl and Cu_3Al are of particular interest since their bulk resistivity is smaller than RuAl: indeed, the increase of resistivity predicted here is obtained considering perfectly diffuse surfaces, while they could be partially reflective. In this case, the increase of resistivity would be smaller than the one reported here, up to zero for perfectly reflective surfaces. Note that for copper + liner, most of the resistivity increase comes from the thickness of the additional liner (distance from pristine copper shown with a star symbol to the purple full line).

Rectangular nanowire resistivity

Equation (5) provides the reduction of electron-phonon scattering time for a thin film, but cannot be straightforwardly applied when the dimensions are shrunk along two directions, like for a rectangular nanowire. We consider here the cases of a rectangular nanowire of thickness h of width $w = 3h$ or $w = h$ (aspect ratio w/h of 1:3 or 1:1, respectively). In these cases, the relaxation times must be corrected to account for confinement effects both along the thickness and the width. Following the derivation provided in Appendix, one finds

$$\tau_{n\mathbf{k}} = \tau_{n\mathbf{k}}^{\text{ep}}\left(1 - R_{\hat{u}} - R_{\hat{s}} + 2R_{\hat{u}}R_{\hat{s}} - \{R_{\hat{s}} - R_{\hat{u}} + 2R_{\hat{u}}R_{\hat{s}}\} \times \exp\left[\frac{-1}{R_{\hat{u}}}\right]\right) \quad \text{if } w|\vec{\boldsymbol{\lambda}}\cdot\hat{u}| \leqslant h|\vec{\boldsymbol{\lambda}}\cdot\hat{s}|$$
$$\tau_{n\mathbf{k}} = \tau_{n\mathbf{k}}^{\text{ep}}\left(1 - R_{\hat{u}} - R_{\hat{s}} + 2R_{\hat{u}}R_{\hat{s}} - \{R_{\hat{u}} - R_{\hat{s}} + 2R_{\hat{u}}R_{\hat{s}}\} \times \exp\left[\frac{-1}{R_{\hat{s}}}\right]\right) \quad \text{if } w|\vec{\boldsymbol{\lambda}}\cdot\hat{u}| > h|\vec{\boldsymbol{\lambda}}\cdot\hat{s}|, \tag{17}$$

where $R_{\hat{u}} = |\vec{\boldsymbol{\lambda}}\cdot\hat{u}|/h$ and $R_{\hat{s}} = |\vec{\boldsymbol{\lambda}}\cdot\hat{s}|/w$, while $\hat{u}$ and $\hat{s}$ are the confinement directions. Taylor expanding the exponential around 0 leads to a new approximation, independent of the electron-phonon lifetime, for the low-dimension resistivity,

$$\tau_{n\mathbf{k}} \approx \frac{h}{2|\vec{\boldsymbol{v}}\cdot\hat{u}|}\left(1 - \frac{h}{w}\frac{|\vec{\boldsymbol{v}}\cdot\hat{u}|}{|\vec{\boldsymbol{v}}\cdot\hat{s}|}\right) + O(h^3) \text{ if } w|\vec{\boldsymbol{v}}\cdot\hat{u}| < h|\vec{\boldsymbol{v}}\cdot\hat{s}|$$
$$\tau_{n\mathbf{k}} \approx \frac{w}{2|\vec{\boldsymbol{v}}\cdot\hat{v}|}\left(1 - \frac{w}{h}\frac{|\vec{\boldsymbol{v}}\cdot\hat{s}|}{|\vec{\boldsymbol{v}}\cdot\hat{u}|}\right) + O(h^3) \text{ if } w|\vec{\boldsymbol{v}}\cdot\hat{u}| > h|\vec{\boldsymbol{v}}\cdot\hat{s}|$$
$$\tau_{n\mathbf{k}} \approx \frac{h}{3|\vec{\boldsymbol{v}}\cdot\hat{u}|} + O(h^4) \text{ if } w|\vec{\boldsymbol{v}}\cdot\hat{u}| = h|\vec{\boldsymbol{v}}\cdot\hat{s}|, \tag{18}$$

compared to the thin film case, the relaxation times -and consequently the conductivity- are reduced whatever the choice of the problem parameters, even in the case where $w|\vec{\boldsymbol{v}}\cdot\hat{u}| = h|\vec{\boldsymbol{v}}\cdot\hat{s}|$ (factor 1/3 in this case versus 1/2 for the thin film case). In principle, a new screening of the materials based on this new quantity should be performed. However, one notes that the additional confinement in-plane is superimposed to the out-of-plane one: the resistivity increase in a rectangular nanowire is always larger than in a thin film of an equivalent thickness, as a consequence of Eq. (18). If the resistivity increase was already bad in the case of a thin film, it will only get worse in the case of a rectangular nanowire. In conse-

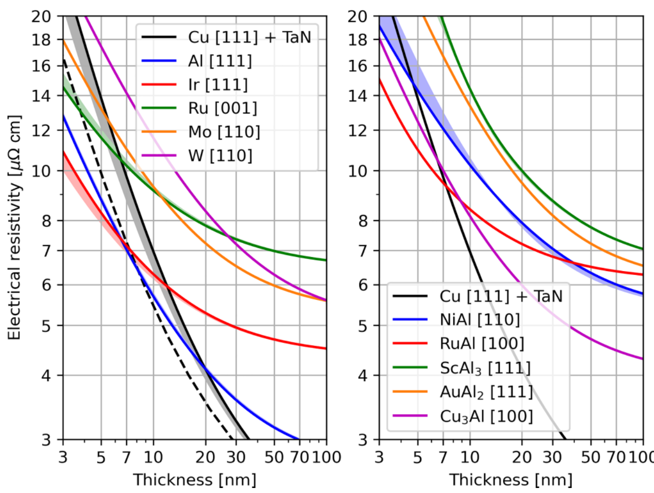

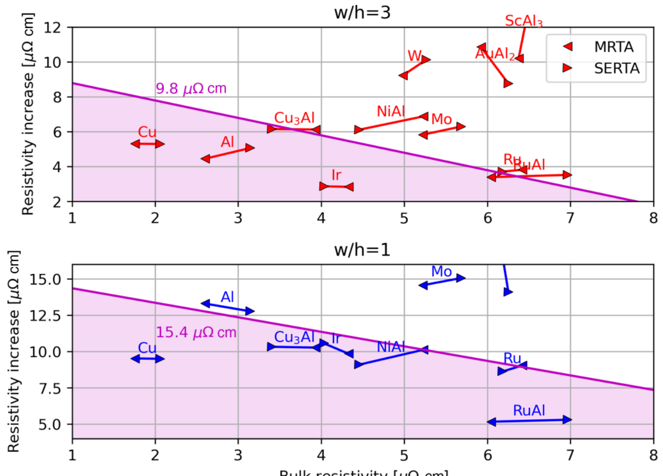

FIG. 6. Variation of the resistivity for nanowires of (left) elementary metals and (right) the most promising binary metals, with respect to their thickness (aspect ratio $w = 3h$). The resistivity variation for the copper +TaN liner in a thin film is shown in dash black for sake of comparison. The shaded areas shows the variation of the curve depending on the confinement direction along the width direction. The thickness of the TaN liner for Cu is 3 nm.

FIG. 7. Comparison of the resistivity increase in nanowire from bulk to 7 nm with respect to the bulk resistivity for two different aspect ratios (top: 1:3, bottom: 1:1). The full line corresponds to the Cu + TaN limit (materials below that line have lower resistivity than Cu + liner).

quence, we limit this additional investigation to the materials that came out from the thin film analysis. We show in Fig. S14 the correlation between the increase of resistivity from bulk to a 7-nm-thick rectangular nanowire and the corresponding $\rho\lambda$ (based on Eq. (18)). They are found to be well correlated in the case of 1:3 aspect ratio, but not as much for 1:1 mostly due to 2 outliers (W and $ScAl_3$). Predictions based on $\rho\lambda$ for this aspect ratio thus would require some precautions.

The results for the resistivity increase for 1:3 rectangular nanowires are shown in Fig. 6, considering either the experimentally known growth orientation, or the one that yields the lowest resistivity increase for binaries. We then consider the in-plane confinement along two different orthogonal crystalline directions: [1-10] and [11-2] for FCC crystals, [101] and [011] for BCC crystals, [100] and [010] for hexagonal crystals, [010] and [001] for SC crystals grown along [100]. We find little variations between these confinement directions as shown in Fig. 6 (shaded areas). Note that this shall however varies depending on the considered aspect ratio (here 1:3).

One can directly see that the crossings between the different resistivity curves that were observed for elementary metals and binaries are reproduced in the case of rectangular nanowires, and they occur at comparable thicknesses than for thin films (~10 nm or smaller). The same binary metals identified based on their thin films resistivity come out from this investigation: RuAl, NiAl and Cu_3Al all turn out to be promising materials for low-dimension interconnects. At 7 nm, only Al, RuAl and Ir theoretically show a resistivity lower than 10 $\mu\Omega$ cm, while Al, Ru, Mo, W, NiAl and $CuAl_3$ all fall below 20 $\mu\Omega$ cm. Depending on the in-plane confinement direction, Cu can also fall below 20 $\mu\Omega$ cm (for the [1-10] confinement orientation). Finally, we reproduce the data at 7 nm in Fig. 7 for both 1:3 and 1:1 aspect ratios and compare them to the bulk resistivity predicted from SERTA and MRTA. The transport direction is taken as [11-2] for FCC crystals, [011] for BCC ones, [100] for HCP crystal, [001] for NiAl, [001] for RuAl and Cu_3Al, [11-2] for $ScAl_3$ and $AuAl_2$ (confinement directions are perpendicular). Overall, the same conclusions can be drawn from this analysis as the ones observed for the thin film: RuAl, NiAl, Al, Cu_3Al, Ir and Ru all show the smallest increase of resistivity, followed by Mo and Cu_3Al. For 1:3 rectangular wires, Ir, Ru and RuAl show the smallest increase, while RuAl clearly stands out for square wires. For other aspect ratios, not investigated in this work, the resistivity increase lies between the results reported here for thin films and the ones for nanowires, provided that the confinement directions with respect to the crystallographic axes are kept the same.

VI. CONCLUSION

In this work, we investigated the evolution of the electrical resistivity of elementary and binary metals in sub-10-nm-thick films, coupling first-principles simulations with the exact resolution of the Boltzmann transport equation in such confined geometries. We first have highlighted the importance of the growth orientation on the resistivity increase at low dimensions, discussing the validity of different approximations to estimate such a change without computing electron-phonon relaxation times. We then evaluated the impact of confinement on binary metals for low-dimension interconnects, both considering thin films and rectangular nanowires. For the latter case, we derived an analytical solution and concluded that RuAl, NiAl, and Cu_3Al all turn out to be interesting candidates for such applications. This however requires validation that their grain scattering contributions can be kept under control experimentally.

In this work, we restricted ourselves to the relaxation-time approximation (SERTA or MRTA) to find a solution to this equation for confined geometries. This however leads to a relatively important uncertainty on the bulk resistivity (~10%). While most recent code developments allow one to solve

iteratively Boltzmann's transport equation considering only phonon as a source of scattering [12], the inclusion at the same time of surface scattering remains to be investigated. A simple way out would be the rescaling of the electron-phonon relaxation time to fit the bulk electrical resistivity from the iterative solution, then apply the analytical expressions (5) and (17) for thin films and rectangular nanowires, respectively. One however approximates in this case the impact of the iterative BTE on the increase of resistivity due to confinement.

Another challenge for a full-scale screening lies in the estimation of the bulk electrical resistivity and its computational cost. Using a variational approach to solve the BTE [45] may allow one to reduce the density of the electron and phonon wave-vector meshes to obtain converged bulk electrical resistivity. However, one would loose information on the wave-vector resolution required to include surface scattering. For this second difficulty, one could use the $\rho\lambda(\hat{u}_n)$ or r_{film} to predict the resistivity increase, with the values provided in this paper. This could allow one to screen materials based on their bulk resistivity and the contribution from surface scattering in a more effective manner.

ACKNOWLEDGMENT

The authors thank the Imec Industrial Affiliation Program (IIAP) on Nano-Interconnects for funding.

APPENDIX

1. Derivation for 2D-confinement Boltzmann's transport equation

To derive the 2D confinement case, we start from Boltzmann's transport equation in the relaxation time approximation:

$$-e\frac{\partial f^0_{n\mathbf{k}}}{\partial \epsilon_{n\mathbf{k}}}\mathbf{v}_{n\mathbf{k}}\cdot\mathbf{E} = \frac{g_{n\mathbf{k}}}{\tau_{n\mathbf{k}}} + \mathbf{v}_{n\mathbf{k}}\cdot\nabla_r g_{n\mathbf{k}} \tag{A1}$$

with $f^0_{n\mathbf{k}}$ is the equilibrium Fermi distribution, $\mathbf{E}$ is the electric field, and $g_{n\mathbf{k}}$ is the perturbation in term of the carrier distribution. We consider here a rectangular wire; at one boundary (that depends on the sign of the velocity), the distribution change must be zero.

For the sake of the derivation, we consider here that the growth orientation of the film is along z (thickness h) and the in-plane confinement is along y (width w); see Fig. 8. The general solutions of this problem are exponential functions, although the corresponding solution space is constrained by the boundary conditions of the problem. We suppose here that the surfaces are fully diffuse, leading to $g(y,0)=0$ and $g(0,z)=0$ for positive velocities (both along y and z). Using the method of characteristics, this downselects the exponential solutions to

$$g^{(A)}_{n\mathbf{k}} = -e\tau_{n\mathbf{k}}\frac{\partial f^0_{n\mathbf{k}}}{\partial \epsilon_{n\mathbf{k}}}\mathbf{v}_{n\mathbf{k}}\cdot\mathbf{E} + u^{(A)}\left(\frac{y}{\lambda_y}-\frac{z}{\lambda_z}\right)\exp\left(\frac{-y}{\lambda_y}\right) \tag{A2}$$

and

$$g^{(B)}_{n\mathbf{k}} = -e\tau_{n\mathbf{k}}\frac{\partial f^0_{n\mathbf{k}}}{\partial \epsilon_{n\mathbf{k}}}\mathbf{v}_{n\mathbf{k}}\cdot\mathbf{E} + u^{(B)}\left(\frac{y}{\lambda_y}-\frac{z}{\lambda_z}\right)\exp\left(\frac{-z}{\lambda_z}\right), \tag{A3}$$

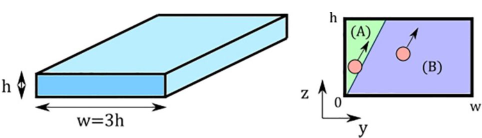

FIG. 8. Schematic representation of the rectangular nanowire structure. It is considered to be infinite along the transport direction (perpendicular to both the width and thickness directions).

where $u^{(A)}(y/\lambda_y - z/\lambda_z)$ are $u^{(B)}(y/\lambda_y - z/\lambda_z)$ integration functions, and where the two different functions correspond to two different domains in space: the former (A) corresponds to the electrons that are coming from the left surface of the wire, while the (B) corresponds to the electrons from the bottom surface. The existence of two domains of solutions directly arises from the shape of the differential equation and from the boundary conditions, the latter imposing no y or z dependency of the solution that would cover the whole spatial domain, i.e., a trivial solution. With two spatial domains that contains only one of the boundary or the other at the time, nontrivial solutions are possible, provided they are exactly matched at the domain separation. From a geometrical inspection of the problem (see Fig. 8), the line that delimits the frontier between these two domains is

$$\frac{y}{\lambda_y} = \frac{z}{\lambda_z} \tag{A4}$$

that either intercepts the right surface at $(w, w\lambda_z/\lambda_y)$ or the top surface at $(h\lambda_y/\lambda_z, h)$, depending on the parameters of the problem: one keeps the solution whose y or z intercept is on the positive axis. At the crossing line between the domains, the distribution of electrons should be continuous, leading to $u^{(A)} = u^{(B)} = e\tau_{n\mathbf{k}}\partial f^0_{n\mathbf{k}}/\partial\epsilon_{n\mathbf{k}}\mathbf{v}_{n\mathbf{k}}\cdot\mathbf{E}$. We are now interested to the current density flowing in the system, supposing that the external electric field is applied along x. The partial contribution of the electron $(n,\mathbf{k})$ to the total current density is

$$j_{n\mathbf{k},x} = \frac{-ev_{n\mathbf{k},x}}{wh}\int_0^w\int_0^h g_{n\mathbf{k}}(y,z)dydz. \tag{A5}$$

This can be solved analytically to find the expression for the relaxation time considering the 2D confinement. Since the separation line between (A) and (B) can intercept either the y and z axes, there are two possible solutions for the relaxation time of the electron $(n,\mathbf{k})$ depending on the different parameters of the problem, namely,

$$\tau_{n\mathbf{k}} = \tau^{\text{ep}}_{n\mathbf{k}}\left(1 - R_z - R_y + 2R_zR_y - \{R_y - R_z + 2R_zR_y\}\times\exp\left[\frac{-1}{R_z}\right]\right) \quad \text{if } w|\lambda_z| \leqslant h|\lambda_y|$$

$$\tau_{n\mathbf{k}} = \tau^{\text{ep}}_{n\mathbf{k}}\left(1 - R_z - R_y + 2R_zR_y - \{R_z - R_y + 2R_zR_y\}\times\exp\left[\frac{-1}{R_y}\right]\right) \quad \text{if } w|\lambda_z| > h|\lambda_y|,$$

where we have introduced $R_y = \lambda_y/w$ and $R_z = \lambda_z/h$ for sake of legibility. If one would consider now both negative and positive components for the electron mean-free path, one can show the above-mentioned solution still works al-

beit that $R_y = |\lambda_y|/w$ and $R_z = |\lambda_y|/w$. In the limit of $h/\lambda_z \to \infty$ or $w/\lambda_y \to \infty$, while keeping the other ratio finite, one recovers Eq. (5), as one would have expected.

[1] D. Gall, The search for the most conductive metal for narrow interconnect lines, J. Appl. Phys. **127**, 050901 (2020).

[2] D. Gall, J. Cha, Z. Chen, H. Han, C. Hinkle, J. Robinson, R. Sundararaman, and R. Torsi, Materials for interconnects, MRS Bull. **46**, 959 (2021), funding Information: This work was supported by IMPACT, a center in nCORE, a Semiconductor Research Corporation (SRC) program, and by NEWLIMITS, a center in nCORE, a SRC program sponsored by the National Institute of Standards and Technology (NIST) through Award No. 70nANB17H041. Publisher Copyright: © 2021, The Author(s), under exclusive licence to The Author(s), under exclusive License to the Materials Research Society.

[3] A. F. Mayadas and M. Shatzkes, Electrical-resistivity model for polycrystalline films: The case of arbitrary reflection at external surfaces, Phys. Rev. B **1**, 1382 (1970).

[4] Y. C. Cho, S. Lee, M. Ajmal, W.-K. Kim, C. R. Cho, S.-Y. Jeong, J. H. Park, S. E. Park, S. Park, H.-K. Pak *et al.*, Copper better than silver: Electrical resistivity of the grain-free single-crystal copper wire, Cryst. Growth Des. **10**, 2780 (2010).

[5] D. Gall, Electron mean free path in elemental metals, J. Appl. Phys. **119**, 085101 (2016).

[6] C. Adelmann, L. G. Wen, A. P. Peter, Y. K. Siew, K. Croes, J. Swerts, M. Popovici, K. Sankaran, G. Pourtois, S. Van Elshocht *et al.*, Alternative metals for advanced interconnects, in *Proceedings of the IEEE International Interconnect Technology Conference* (IEEE, New York, 2014), pp. 173–176.

[7] S. Dutta, K. Sankaran, K. Moors, G. Pourtois, S. Van Elshocht, J. Bömmels, W. Vandervorst, Z. Tőkei, and C. Adelmann, Thickness dependence of the resistivity of platinum-group metal thin films J. Appl. Phys. **122**, 025107 (2017).

[8] K. Sankaran, S. Clima, M. Mees, and G. Pourtois, Exploring alternative metals to Cu and W for interconnects applications using automated first-principles simulations, ECS J. Solid State Sci. Technol. **4**, N3127 (2015).

[9] S. Kumar, C. Multunas, B. Defay, D. Gall, and R. Sundararaman, Ultralow electron-surface scattering in nanoscale metals leveraging Fermi-surface anisotropy, Phys. Rev. Mater. **6**, 085002 (2022).

[10] K. Sankaran, K. Moors, Z. Tőkei, C. Adelmann, G. Pourtois, Ab initio screening of metallic MAX ceramics for advanced interconnect applications, Phys. Rev. Mater. **5**, 056002 (2021).

[11] S. Poncé, W. Li, S. Reichardt, and F. Giustino, First-principles calculations of charge carrier mobility and conductivity in bulk semiconductors and two-dimensional materials, Rep. Prog. Phys. **83**, 036501 (2020).

[12] R. Claes, G. Brunin, M. Giantomassi, G.-M. Rignanese, and G. Hautier, Assessing the quality of relaxation-time approximations with fully automated computations of phonon-limited mobilities, Phys. Rev. B **106**, 094302 (2022).

[13] S. Poncé, E. Margine, C. Verdi, and F. Giustino, EPW: Electron-phonon coupling, transport and superconducting properties using maximally localized Wannier functions, Comput. Phys. Commun. **209**, 116 (2016).

[14] J.-J. Zhou, J. Park, I.-T. Lu, I. Maliyov, X. Tong, and M. Bernardi, Perturbo: A software package for ab initio electron–phonon interactions, charge transport and ultrafast dynamics, Comput. Phys. Commun. **264**, 107970 (2021).

[15] X. Gonze, G.-M. Rignanese, M. Verstraete, J.-M. Beuken, Y. Pouillon, R. Caracas, F. Jollet, M. Torrent, G. Zerah, M. Mikami *et al.*, A brief introduction to the ABINIT software package, Z. Kristallogr. **220**, 558 (2005).

[16] X. Gonze, B. Amadon, P.-M. Anglade, J.-M. Beuken, F. Bottin, P. Boulanger, F. Bruneval, D. Caliste, R. Caracas, M. Côté *et al.*, ABINIT: First-principles approach to material and nanosystem properties, Comput. Phys. Commun. **180**, 2582 (2009).

[17] X. Gonze, F. Jollet, F. A. Araujo, D. Adams, B. Amadon, T. Applencourt, C. Audouze, J.-M. Beuken, J. Bieder, A. Bokhanchuk *et al.*, Recent developments in the ABINIT software package, Comput. Phys. Commun. **205**, 106 (2016).

[18] X. Gonze *et al.*, The Abinit project: Impact, environment and recent developments, Comput. Phys. Commun. **248**, 107042 (2020).

[19] G. Brunin, H. P. C. Miranda, M. Giantomassi, M. Royo, M. Stengel, M. J. Verstraete, X. Gonze, G.-M. Rignanese, and G. Hautier, Phonon-limited electron mobility in Si, GaAs, and GaP with exact treatment of dynamical quadrupoles, Phys. Rev. B **102**, 094308 (2020).

[20] G. Brunin, H. P. C. Miranda, M. Giantomassi, M. Royo, M. Stengel, M. J. Verstraete, X. Gonze, G.-M. Rignanese, and G. Hautier, Electron-Phonon beyond Fröhlich: Dynamical Quadrupoles in Polar and Covalent Solids, Phys. Rev. Lett. **125**, 136601 (2020).

[21] Z. Tong, S. Li, X. Ruan, and H. Bao, Comprehensive first-principles analysis of phonon thermal conductivity and electron-phonon coupling in different metals, Phys. Rev. B **100**, 144306 (2019).

[22] Y. Chen, J. Ma, and W. Li, Understanding the thermal conductivity and Lorenz number in tungsten from first principles, Phys. Rev. B **99**, 020305(R) (2019).

[23] S. Wen, J. Ma, A. Kundu, and W. Li, Large lattice thermal conductivity, interplay between phonon-phonon, phonon-electron, and phonon-isotope scatterings, and electrical transport in molybdenum from first principles, Phys. Rev. B **102**, 064303 (2020).

[24] Y. Hu, S. Li, and H. Bao, First-principles based analysis of thermal transport in metallic nanostructures: Size effect and Wiedemann-Franz law, Phys. Rev. B **103**, 104301 (2021).

[25] M. De Clercq, K. Moors, K. Sankaran, G. Pourtois, S. Dutta, C. Adelmann, W. Magnus, and B. Sorée, Resistivity scaling model for metals with conduction band anisotropy, Phys. Rev. Mater. **2**, 033801 (2018).

[26] K. Moors, K. Sankaran, G. Pourtois, and C. Adelmann, First-principles-based screening method for resistivity scaling of anisotropic metals, Phys. Rev. Mater. **6**, 123804 (2022).

[27] K. Fuchs, The conductivity of thin metallic films according to the electron theory of metals, Math. Proc. Cambridge Philos. Soc. **34**, 100 (1938).

[28] E. Sondheimer, The mean free path of electrons in metals, Adv. Phys. **1**, 1 (1952).

[29] C. Kittel, *Introduction to Solid State Physics,* 5th ed. (John Wiley & Sons, Hoboken, NJ, 1976).

[30] A. H. Romero, D. C. Allan, B. Amadon, G. Antonius, T. Applencourt, L. Baguet, J. Bieder, F. Bottin, J. Bouchet, E. Bousquet *et al.*, ABINIT: Overview and focus on selected capabilities, J. Chem. Phys. **152**, 124102 (2020).

[31] D. R. Hamann, Optimized norm-conserving Vanderbilt pseudopotentials, Phys. Rev. B **88**, 085117 (2013).

[32] M. van Setten, M. Giantomassi, E. Bousquet, M. Verstraete, D. Hamann, X. Gonze, and G.-M. Rignanese, The PseudoDojo: Training and grading a 85 element optimized norm-conserving pseudopotential table, Comput. Phys. Commun. **226**, 39 (2018).

[33] See Supplemental Material at http://link.aps.org/supplemental/10.1103/PhysRevB.108.125117 for convergence studies, phonon band structures, and additional figures that are not crucial for the understanding of the manuscript.

[34] J. Y. Kim, M.-W. Oh, S. Lee, Y. C. Cho, J.-H. Yoon, G. W. Lee, C.-R. Cho, C. H. Park, and S.-Y. Jeong, Abnormal drop in electrical resistivity with impurity doping of single-crystal Ag, Sci. Rep. **4**, 5450 (2014).

[35] K. L. Chopra, L. C. Bobb, and M. H. Francombe, Electrical resistivity of thin single-crystal gold films, J. Appl. Phys. **34**, 1699 (1963).

[36] R. Lapovok, Y. Amouyal, Y. Qi, A. Berner, A. Kosinova, E. Lakin, D. A. Molodov, and E. Zolotoyabko, Enhancement of electrical conductivity in aluminum single crystals by boron treatment in solid state, J. Mater. Sci. **55**, 2564 (2020).

[37] R. A. Holmwood and R. Glang, Resistivity and temperature coefficient of pure molybdenum, J. Chem. Eng. Data **10**, 162 (1965).

[38] D. Choi and K. Barmak, On the potential of tungsten as next-generation semiconductor interconnects, Electron. Mater. Lett. **13**, 449 (2017).

[39] R. W. Powell, R. P. Tye, and M. J. Woodman, The thermal conductivity and electrical resistivity of polycrystalline metals of the platinum group and of single crystals of ruthenium, J. Less-Common Met. **12**, 1 (1967).

[40] S. Poncé, F. Macheda, E. R. Margine, N. Marzari, N. Bonini, and F. Giustino, First-principles predictions of Hall and drift mobilities in semiconductors, Phys. Rev. Res. **3**, 043022 (2021).

[41] A. Togo and I. Tanaka, `Spglib`: A software library for crystal symmetry search, arXiv:1808.01590.

[42] H. Nie, S. Xu, S. Wang, L. You, Z. Yang, C. Ong, J. Li, and T. Liew, Structural and electrical properties of tantalum nitride thin films fabricated by using reactive radio-frequency magnetron sputtering, Appl. Phys. A **73**, 229 (2001).

[43] A. Jain, S. P. Ong, G. Hautier, W. Chen, W. D. Richards, S. Dacek, S. Cholia, D. Gunter, D. Skinner, G. Ceder *et al.*, Commentary: The Materials Project: A materials genome approach to accelerating materials innovation, APL Mater. **1**, 011002 (2013).

[44] Y. Li and J. Zhu, L1-Norm quantile regression, J. Comput. Graph. Stat. **17**, 163 (2008).

[45] B. Xu and M. J. Verstraete, First Principles Explanation of the Positive Seebeck Coefficient of Lithium, Phys. Rev. Lett. **112**, 196603 (2014).